Chemical Physics Letters xxx (2013) xxx–xxx

Contents lists available at SciVerse ScienceDirect

Chemical Physics Letters

journal homepage: www.elsevier.com/locate/cplett

Vibrational predissociation spectroscopy of Ar-tagged, trisubstituted silyl cations

Andrew F. DeBlase [a], Michael T. Scerba [b], Thomas Lectka [b], Mark A. Johnson [a,*]

[a] Sterling Chemistry Laboratory, Yale University, P.O. Box 208107, New Haven, CT 06520, USA
[b] Department of Chemistry, Johns Hopkins University, 3400 North Charles Street, Baltimore, MD 21218, USA

ARTICLE INFO

Article history:
Available online xxxx

ABSTRACT

Vibrational predissociation spectra of the $(CH_3)_2RSi^+ \cdot Ar_n$, (R = H and CH_3, n = 1 and 2) ions are compared with harmonic calculations to structurally characterize these putative reactive intermediates. Although the vibrational photofragmentation behavior indicates that the Ar–Si bond is quite strong relative to that found in closed shell ions, formation of the Ar adducts is calculated to cause only minor perturbations to the intrinsic vibrational band patterns of the isolated ions. In both (R = H and CH_3) cases, the vibrational spectra are very simple, consisting entirely of sharp features readily assigned to fundamentals anticipated by their harmonic spectra.

1. Introduction

Silyl cations are the third-row analogues of the familiar carbocations. Here we are concerned with the trisubstituted silyl cations (R_3Si^+), which have proven difficult to characterize in the condensed phase because they bind strongly to solvents and counterions [1,2]. In our approach, two silyl cations, [$(CH_3)_2HSi^+$ and $(CH_3)_3Si^+$], are isolated in the gas phase and complexed with weakly bound Ar atoms. The vibrational spectra of these complexes are then recorded using mass-selective vibrational predissociation over the range of 600–3500 cm^{-1}. The vibrational band patterns are analyzed in the context of harmonic spectra calculated for minimum energy structures, which predict Ar attachment to occur preferentially to Si roughly along the axis perpendicular to the plane of the tricoordinated ions [3,4]. This arrangement results in a slight pyramidal deformation of the core SiR_3^+ structure as depicted in Figure 1.

This study closely follows previous reports in which vibrational predissociation was used to determine the structures of the Ar complexes with carbocations [5] (e.g., CH_3^+ [6], arenium ions [7], tert-butyl cation [8], and the allyl and 2-propenyl cations [9]). A key observation from those earlier investigations is that, although Ar attachment is often used as a weakly bound mass 'messenger' to allow spectroscopic characterization of mass-selected ions [10–12], some carbocations bind the first few Ar atoms sufficiently strongly to distort their molecular frameworks [6]. For example, thermochemical measurements [13] for gas phase clustering of CH_3^+ with Ar yield a binding enthalpy ($\Delta H°$) of 3950 ± 700 cm^{-1}. While the binding energy of a second Ar atom to CH_3^+ ($\Delta H°$ = 790 ± 70 cm^{-1}) does decrease significantly relative to the first, even that value is qualitatively larger than typically observed for closed shell molecular cations in the same size range (e.g., ~500 cm^{-1} for Ar binding to $PhCO^+$) [14]. The CH_3^+ ion was found to attach the first Ar atom along the C_3 axis similar to the arrangement depicted in Figure 1, thus lowering the overall symmetry from D_{3h} to C_{3v}. Interestingly, D_{3h} symmetry is not restored when a second Ar attaches at the opposite side of the carbon (i.e., one of the two Ar atoms is closer to the central C than the other). Spectral consequences of argon attachment to CH_3^+ are the blue shift of the asymmetric CH stretching (ν_3) transition by 37 and 44 cm^{-1} for the first and second Ar atoms, respectively [6,15,16].

Because silicon has the capability of expanding its valence to form pentacoordinate complexes [17], it can be anticipated that highly electrophilic sp^2 silyl cations are strongly perturbed by nucleophilic species in solution that can bind at the axial positions of a triganal bipyramid. Indeed, in contrast to their carbocation analogues, attempts to generate free *alkylsilyl* cations of any sort in solution have been met with frustration and disappointment. Recent attempts to isolate silyl cations in solution include complexation with weakly coordinating counter-anions [18] combined with the introduction of bulky, resonance-stabilizing substituents such as mesityl. For example, Lambert reported the synthesis of trimesitylsilyl cation in the presence of the TPFBP anion with benzene as a solvent [19], and established the silyl cation structure through theoretical analysis of the experimental ^{29}Si NMR chemical shifts. In another approach, Mihalic and coworkers [20] used matrix isolation infrared spectroscopy to prepare and study vibrationally cold intermediates in the reaction of trimethylsilylacetylenes with antimony pentaflouride. The key species were formed by reheating the matrix, however, and the resulting spectra were admixtures of many products, thus preventing definitive assignment of spectral signatures associated with the silyl cation.

* Corresponding author. Fax: +1 203 432 6144.
E-mail address: mark.johnson@yale.edu (M.A. Johnson).

0009-2614/$ - see front matter © 2013 Elsevier B.V. All rights reserved.
http://dx.doi.org/10.1016/j.cplett.2013.03.002

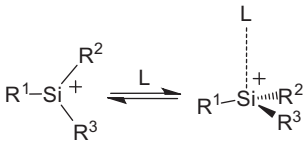

Figure 1. Structure of the complex formed between a trisubstituted silyl cation and a weakly binding ligand (L).

Detailed studies of a silyl ion isolated in the gas phase have been carried out on the SiH_3^+ ion, which employed a variety of tools including photoelectron, [21] photoionization [22], Rydberg [23] and velocity-modulation infrared [24] spectroscopies. All results are consistent with the planar structure determined by analysis of the rotationally resolved out-of-plane Si–H bending fundamental (ν_2) [24]. Very recently, Dopfer and coworkers [25,26] have successfully applied Ne predissociation spectroscopy to study the Si–H–Si bridge in $Si_2H_7^+$, an interesting species from the perspective of H-passivation at the surface of Si_n clusters. Features were observed as low as 750 cm^{-1} with minor shifts (mostly < 10 cm^{-1}) from the rare gas tag. Here we extend this gas phase work to di- and tri-substituted silyl cations [$(CH_3)_3Si^+$ and $(CH_3)_2HSi^+$] using vibrational predissociation spectrometry of the mass-selected Ar adducts. We will show that the experimental vibrational band patterns of these species are both remarkably simple and very accurately explained by theoretical predictions at the harmonic level. The fact that the same level of calculation also predicts only minor shifts upon Ar attachment suggests that the reported spectra are useful representations of the bare ion behaviors.

2. Results and discussion

2.1. Preparation of $(CH_3)_3Si^+ \cdot Ar_n$ and $(CH_3)_2HSi^+ \cdot Ar_n$ and details of spectrometer

Vibrational predissociation spectra of the $(CH_3)_2RSi^+ \cdot Ar_n$ [R = H and CH_3, n = 1 and 2] complexes were obtained using the Yale double focusing, tandem time-of-flight photofragmentation spectrometer described previously [27]. The $(CH_3)_2HSi^+$ and $(CH_3)_3Si^+$ ions were generated by 1 keV electron impact ionization of an Ar supersonic expansion containing trace $[(CH_3)_2HSi]_2$, which was entrained into the main expansion through a second pulsed valve [28]. The ion distribution is dominated by the homogeneous Ar_n^+ cluster distribution, and it is typical under these conditions that the Si-based product ions are formed by Ar cluster-mediated charge transfer [29,30]:

$$[(CH_3)_2HSi]_2 + Ar_n^+ \rightarrow [(CH_3)_2HSi]_2 \cdot Ar_n^+ \rightarrow (CH_3)_2HSi^+ \cdot Ar_{n-m} + (CH_3)_2HSi + mAr \quad (1)$$

$$[(CH_3)_2HSi]_2 + Ar_n^+ \rightarrow [(CH_3)_2HSi]_2 \cdot Ar_n^+ \rightarrow (CH_3)_3Si^+ \cdot Ar_{n-m} + CH_3H_2Si \cdot + mAr \quad (2)$$

The precursor $[(CH_3)_2HSi]_2$ compound could either be present in the neutral Ar_n cluster at the time of ionization or collide with an already formed Ar_n^+ cluster, as stressed by Eqs. (1) and (2). Either way, the product ions retain several Ar atoms as illustrated in a typical mass spectrum displayed in Figure 2, and achieve an internal energy consistent with that expected for the evaporative ensemble [31]. In addition to the parent ion, ($[(CH_3)_2HSi]_2^+$, teal), the two dominant Si-based ions in the product distribution result from fission of the Si–Si bond (Eqs. (1) and (2), second step). The [$(CH_3)_3Si^+$, red] fragment appears to be formed by transfer from one of the methyl groups to the other Si atom, while $(CH_3)_2HSi^+$ (blue) formation results from retention of the methyl. We also observed fragments corresponding to loss of a hydrogen atom ($Si_2H(CH_3)_4^+$, turquoise) and loss of a methyl group ($Si_2H_2(CH_3)_3^+$, green) from the disilyl parent compound. The peaks marked by (∗) in Figure 2 indicate the specific Ar adducts of primary interest in this Letter.

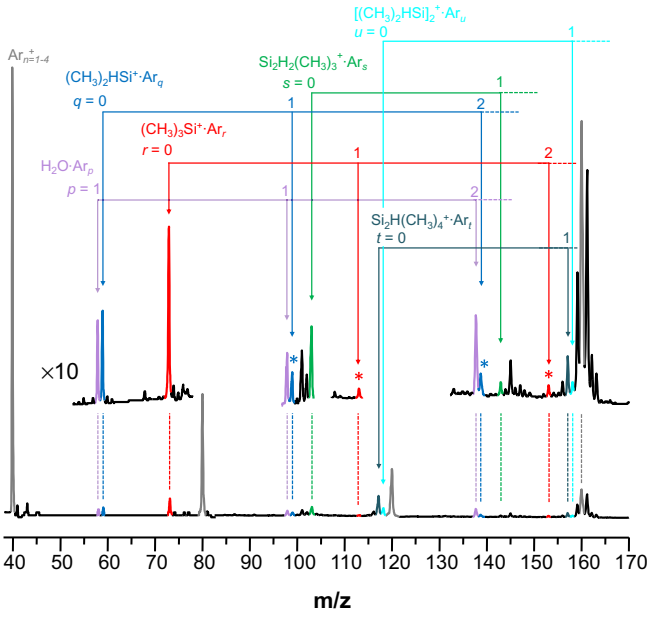

Figure 2. Mass spectrum of 1,1,2,2-tetramethyldisilane $[(CH_3)_2HSi]_2$ vapor entrained into an ionized free jet expansion of argon. The colored peaks highlight the fragment ions and their corresponding Ar adducts. Grey peaks indicate Ar_n^+ clusters. The inset displays an expanded scale (10×) to highlight the relative populations of the ions of interest, with ∗ indicating the m/z species whose vibrational predissociation spectra are reported here. The $H_2O^+ \cdot Ar_n$ distribution arises from water impurity in the beam, verified by its infrared spectrum.

2.2. Calculated structures

To gauge the expected spectral patterns of the binding sites, we carried out electronic structure calculations at the MP2/aug-cc-pVDZ level using the Gaussian 09 suite of programs [32]. Figure 3b and c compare the minimum energy structures found for the bare ions with those obtained for the adducts. Specific parameters for all systems are collected in Table 1. The minimum energy geometries feature Ar attachment directly to the Si charge center as was the case in carbocations such as CH_3^+ [6]. This causes the core silyl cations to adopt slightly distorted trigonal pyramidal configurations. Although addition of a second argon atom occurs at the opposite side of the silicon in a location similar to that of the first, a slight perturbation from planarity is retained (that is, the second Ar binding site is distinct from the first, being more distant from the Si atom (i.e., $r_1 < r_2$)). Figure 3b and c indicate that Ar attachment is calculated to change the Si–C and Si–H bond lengths by less than 0.01 Å, and this minimal perturbation of the intrinsic structures of the core ions is reflected in the fact that the calculated harmonic spectra are not qualitatively perturbed by the tags (see Figure 4). We note that the calculations also predict subtle changes in the rotation of the methyl groups upon addition of the Ar atom (i.e., changing the point groups as indicated in Figure 3b and c). Unfortunately, these effects are not clearly reflected in the spectra, and we therefore cannot reach definite conclusions regarding these predictions.

2.3. Comparison of harmonic predictions with experimental vibrational predissociation spectra

2.3.1. $(CH_3)_3Si^+ \cdot Ar_{1,2}$

The vibrational spectra of the ions provide a quantitative experimental observable that can be directly compared with our

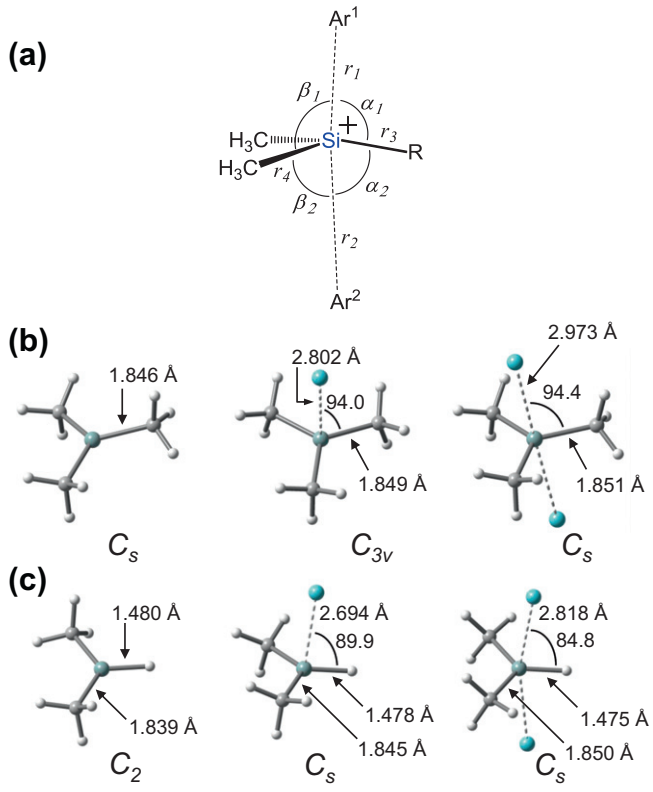

Figure 3. Geometric parameters associated with argon attachment to trisubstituted silyl cations (a) and structures of $(CH_3)_3Si^+{\cdot}Ar_n$ (b) and $(CH_3)_2HSi^+{\cdot}Ar_n$ (c) silyl cations optimized at the MP2/aug-cc-pVDZ level. Point groups are indicated below each structure in italics.

Table 1
Calculated (MP2/aug-cc-pVDZ) geometric parameters[a] for $(CH_3)_3Si^+{\cdot}Ar_n$ and $(CH_3)_2HSi^+{\cdot}Ar_n$ (n = 0, 1 and 2).

R	n_{Ar}	r_1	r_2	r_3	r_4	α_1	α_2	β_1	β_2
CH_3	0	–	–	1.846	1.846	–	–	–	–
CH_3	1	2.801	–	1.849	1.849	94.0	–	94.0	–
CH_3	2	2.973	3.139	1.851	1.851	94.4	84.5	89.0	91.5
H	0	–	–	1.480	1.839	–	–	–	–
H	1	2.694	–	1.478	1.845	89.9	–	95.8	–
H	2	2.818	2.946	1.475	1.850	84.8	81.2	93.6	93.2

[a] Distances (r_1 and r_2) are given in Å and angles (α_1, α_2, β_1, and β_2) are given in degrees and are defined in Figure 3.

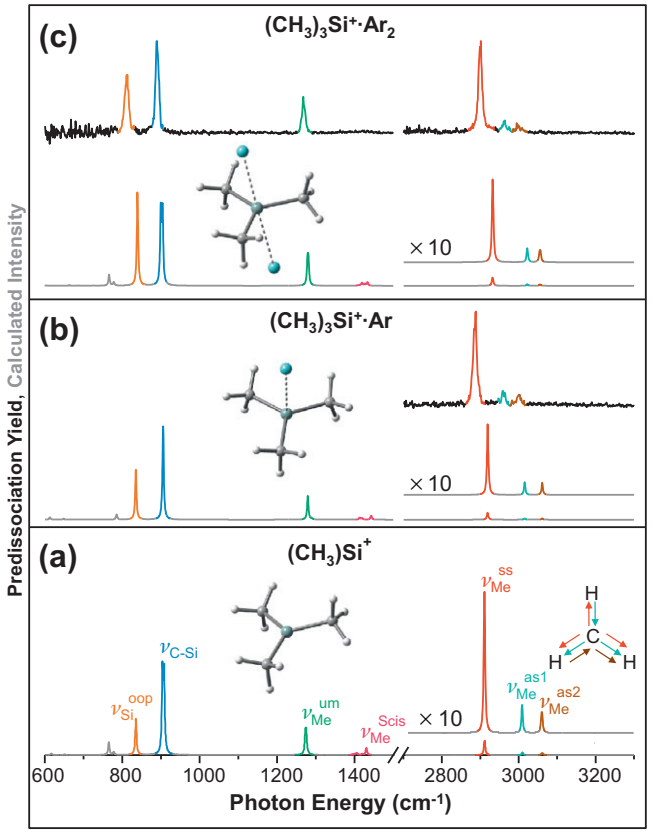

Figure 4. Calculated harmonic spectrum of bare $(CH_3)_3Si^+$ (a) and the vibrational predissociation (black traces) as well as calculated harmonic (grey traces) spectra for $(CH_3)_3Si^+$ cations tagged with one (b) and two (c) argon atoms. The predissociation spectra were obtained by monitoring the photofragmentation of one argon atom below 1500 cm^{-1} and two argon atoms above 1500 cm^{-1}. Harmonic frequencies are at the MP2/aug-cc-pVDZ level (scaled by 0.959 above 2400 cm^{-1} and unscaled below 2400 cm^{-1}). Peaks are color-coded according to their normal mode assignments based on calculated displacements as follows: silicon out-of-plane bend (ν_{Si}^{oop}, orange), C–Si stretch (ν_{C-Si}, blue), methyl scissors (ν_{Me}^{Scis}, pink), methyl umbrella bend (ν_{Me}^{um}, green), methyl symmetric stretch (ν_{Me}^{ss}, red), type-1 methyl asymmetric stretch (ν_{Me}^{as1}, light blue), and type-2 methyl asymmetric stretch (ν_{Me}^{as2}, brown). Motions of the methyl groups associated with the symmetric and types-1 and 2 asymmetric stretches are illustrated in the bottom right hand corner of (a) by the directions of the color coded arrows. Experimental spectra in the regions above and below the break were separately normalized to the most intense peak in each region. Calculated intensities were divided by their frequencies to make them directly comparable with the experimental intensities, which are normalized by laser energy per pulse rather than to the number of photons. The calculated transitions were convoluted with Lorentzians to a full width at half maximum (FWHM) of 4 cm^{-1} and normalized with the most intense transition in the region shown. Calculated CH stretching regions are magnified 10×. (For interpretation of the references to color in this figure legend, the reader is referred to the web version of this article.)

theoretical predictions for the structures. Because single photon predissociation was not observed below 1500 cm^{-1} in the case of $(CH_3)_3Si^+{\cdot}Ar$, and as the second ligand is often more weakly bound than the first, we next turned to the $(CH_3)_3Si^+{\cdot}Ar_2$ cluster to obtain the full spectrum over the laser scan range. One of the two Ar atoms was indeed observed to be photoejected upon excitation down to 811 cm^{-1}. Figure 4 compares the calculated harmonic spectrum of bare $(CH_3)_3Si^+$ (Figure 4a) to the calculated harmonic and predissociation spectra of the one- and two-Ar adducts of $(CH_3)_3Si^+$ in Figure 4b and c, respectively. For the bands that are found in both adducts in the higher energy region, we note that the incremental solvation shifts are very small (<5 cm^{-1}). Although this suggests that Ar attachment does not strongly affect the intrinsic spectrum of the silyl ion, this result does not rule out a scenario where the first Ar could be much more strongly interacting and structurally perturbing than the second. The fact that the calculated spectra agree very well with the experimental pattern for both n = 1 and 2, however, indicates that this level of theory is sufficiently accurate to also predict the behavior of the bare ion. That spectrum (Figure 4a) is also quite similar to the calculated Ar tagged patterns for both n = 1 and 2, and we therefore conclude that Ar attachment does not cause significant distortions for this species. In particular, the calculated shifts in fundamentals are 7 cm^{-1} for the methyl symmetric (ν_{Me}^{ss}) CH stretch, and 5 and 1 cm^{-1} for the two asymmetric CH stretches, respectively. The latter bands are labeled (ν_{Me}^{as1}) and (ν_{Me}^{as2}) at the right in Figure 4a, along with the displacement vectors to illustrate the differences between the modes. We discuss the origin of this splitting below.

The $(CH_3)_3Si^+{\cdot}Ar_2$ spectrum consists of only four intense sharp bands widely dispersed throughout the region that are accurately predicted by the harmonic calculations (lower panels in 4a and 4b). As such, the harmonic spectrum provides an effective

assignment by inspection, and we have color-coded the bands in Figure 4 to emphasize the qualitative character of the dominant displacements at play for each calculated fundamental. The calculated and experimental band positions are collected in Table 2.

The simplicity of the $(CH_3)_3Si^+{\cdot}Ar_2$ spectrum reflects the fact that the three methyl groups are in very similar environments, resulting in several nearly degenerate sets of bands derived from in- and out-of-phase collective vibrations of the modes expected for a single methyl group (e.g., umbrella, symmetric C–H stretch, etc.). The highest energy fundamentals near 3000 cm^{-1} are due to the CH stretching bands which, at this resolution (i.e., the theoretical harmonic spectrum is convoluted with Lorentzians to a FWHM of 4 cm^{-1}), appear as a dominant band at 2888 cm^{-1} with two weaker resonances above it. From the calculations, the strongest feature is traced to three closely spaced transitions arising from the symmetric CH stretching modes on each methyl (ν_{Me}^{ss}, red), while the two weaker bands toward higher energy are derived from close triplets associated with the asymmetric CH stretches [ν_{Me}^{as1} (turquoise) and ν_{Me}^{as2} (brown)]. Of the three transitions contributing to the most intense band, the two nearly degenerate (splitting <1 cm^{-1}), out-of-phase combinations (e.g., two out and one in) of symmetric stretching motions on different methyl groups carry most of the oscillator strength. Interestingly, a similar band pattern was reported by Douberly et al. [8] who obtained the vibrational predissociation spectrum of the tert-butyl cation that contained a dominant band at 2834 cm^{-1} with weaker bands at 2965 and 3036 cm^{-1}.

The weaker two CH peaks at 2964 cm^{-1} (turquoise) and 2995 cm^{-1} (brown) are also of interest, as the small splitting between them encodes the degree to which the methyl groups adopt asymmetrical (i.e., not C_{3v} respect to the Si–C axis) local environments. That is, free rotor methyl groups, such as that in CH_3Cl, would have degenerate *e* symmetry modes. Three of these would give rise to six closely spaced lines that would appear as a single peak like the situation with the symmetric CH stretches. This symmetry is calculated to be broken even in the case of the bare ion, and the effect is enhanced by Ar attachment, resulting in non-equivalent environments of the three methyl H atoms. Although the calculated splitting in $(CH_3)_3Si^+{\cdot}Ar$ between ν_{Me}^{ss} and ν_{Me}^{as1} (96 cm^{-1}) is greater than the experimental result (71 cm^{-1}), the intensities and splitting pattern are in qualitative agreement with the experiment.

Toward the lower energy end of the spectrum, the three predicted transitions from the methyl umbrella modes (ν_{Me}^{um}) appear as a single isolated peak at 1268 cm^{-1}, while the weak HCH bends at 1408–1427 cm^{-1} are barely evident at the present signal-to-noise. Lowest in energy lies a strong doublet with components at 811 cm^{-1} (orange) and 890 cm^{-1} (blue). These are accurately reproduced in the harmonic spectrum, where the normal modes primarily involve displacements of the central Si atom. The lower energy transition at 811 cm^{-1} is thus traced to the non-degenerate, out-of-plane motion (ν_{Si}^{oop}) while the 890 cm^{-1} feature primarily involves the nearly degenerate, in-plane displacements along the Si–C stretching degrees of freedom (ν_{C-Si}).

2.3.2. $(CH_3)_2HSi^+{\cdot}\ Ar_{1,2}$

Having established the assignments of the trimethyl derivative, we next follow the evolution of the bands when the symmetry is lowered by replacing one of the methyl groups with a hydrogen atom in the $(CH_3)_2HSi^+$ ion. In this modification, one might suspect that removal of the bulky methyl group might allow closer interaction with the Si charge center. Indeed, the photophysical behavior indicates that the first Ar atom is significantly more strongly bound, as no fragmentation was observed over the entire range, including upon excitation of the strong 2909 cm^{-1} CH stretching band (red band labeled ν_{Me}^{ss} in the lower trace of Figure 5a/b), which is evident in the $n = 2$ spectrum displayed in Figure 5a. Accurate calculation of the binding energies of the Ar atoms would require substantially higher levels of theory than used to account for the spectra, and we therefore concentrate here on the agreement of the spectra with harmonic predictions for the local minima and point out the approximate binding behavior as a guide for future work on these interesting systems.

The $(CH_3)_2HSi^+{\cdot}Ar_2$ spectrum (Figure 5) is again very simple in that nearly all observable bands are readily assigned to calculated fundamentals for the structure displayed in the lower panel of Figure 5. Note the new sharp band arising from the Si–H stretching fundamental (ν_{SiH}^{s}, maroon) at 2270 cm^{-1}. As before, the strongest bands are often unresolved multiplets due to the collective motion of the two pendant methyl groups as indicated in Table 2. In contrast to the behavior of $(CH_3)_3Si^+{\cdot}Ar_2$, the CH scissors (ν_{Me}^{Scis}) band

Table 2
Experimental (±4 cm^{-1}) and calculated vibrational fundamentals (cm^{-1}) and Intensities (km mol^{-1} in parentheses) for $(CH_3)_3Si^+{\cdot}Ar_n$ and $(CH_3)_2HSi^+{\cdot}Ar_n$ ($n = 0$, 1 and 2).

		$(CH_3)_3Si^+$	$(CH_3)_3Si^+{\cdot}Ar$	$(CH_3)_3Si^+{\cdot}Ar_2$	$(CH_3)_2HSi^+$	$(CH_3)_2HSi^+{\cdot}Ar$	$(CH_3)_2HSi^+{\cdot}Ar_2$
ν_{Me}^{ss}	Exp.	–	2888	2901	–	–	2909
	Calc.	2911 (36), 2912 (40), 2915 (0.61)	2919 (24), 2919 (24), 2922 (4.8)	2931 (21), 2932 (11), 2933 (9.7)	2909 (65), 2911 (6.0)	2918 (34), 2920 (12)	2936 (25), 2937 (8.3)
ν_{Me}^{as1}	Exp.	–	2959	2964	–	–	3004
	Calc.	3009 (5.3), 3009 (0.52), 3010 (9.2)	3015 (0.22), 3015 (0.22), 3015 (8.9)	3021 (0.01), 3022 (5.5), 3023 (1.4)	2999 (0.02), 2999 (21)	3015 (0.98), 3016 (9.9)	3061 (8.3), 3061 (1.9)
ν_{Me}^{as2}	Exp.	–	3003	2995	–	–	2967
	Calc.	3060 (6.5), 3061 (0.45), 3062 (7.0)	3060 (0.02), 3061 (4.5), 3061 (4.5)	3054 (3.2), 3055 (0.83), 3057 (3.6)	3064 (4.6), 3064 (12)	3062 (2.9), 3063 (8.6)	3024 (0.00), 3025 (6.9)
ν_{Me}^{Scis}	Exp.	–	–	1408–1427	–	–	1370–1430
	Calc.	1359 (1.0), 1403 (3.0), 1408 (4.3), 1412 (0.15), 1421 (2.5), 1432 (18)	1389 (0.00), 1413 (3.3), 1413 (3.3), 1419 (2.4), 1419 (2.4), 1443 (15)	1408 (0.98), 1416 (1.1), 1419 (3.0), 1419 (3.4), 1427 (3.8), 1434 (7.8)	1394 (1.6), 1398 (5.5), 1410 (2.3), 1416 (12)	1403 (1.1), 1413 (0.11), 1414 (9.7), 1432 (8.6)	1410 (0.05), 1415 (0.21), 1422 (11), 1434 (6.1)
ν_{Me}^{um}	Exp.	–	–	1268	–	–	1274
	Calc.	1274 (39), 1276 (41), 1282 (1.4)	1279 (38), 1270 (38), 1289 (3.3)	1279 (43), 1281 (42), 1289 (0.17)	1270 (50), 1275 (4.9)	1280 (38), 1285 (11)	1283 (35), 1287 (18)
ν_{C-Si}	Exp.	–	–	890	–	–	923
	Calc.	904 (121), 908 (118)	906 (105), 906 (105)	900 (97), 904 (96)	945 (153)	938 (138)	930 (129)
ν_{Si}^{oop}	Exp.	–	–	811	–	–	822
	Calc.	835 (51)	835 (103)	839 (118)	845 (51)	843 (128)	852 (169)
ν_{Me}^{wag}	Exp.	–	–	–	–	–	858
	Calc.	–	–	–	882 (60)	886 (50)	882 (47)
ν_{SiH}^{s}	Exp.	–	–	–	–	–	2270
	Calc.	–	–	–	2243 (17)	2248 (19)	2259 (20)

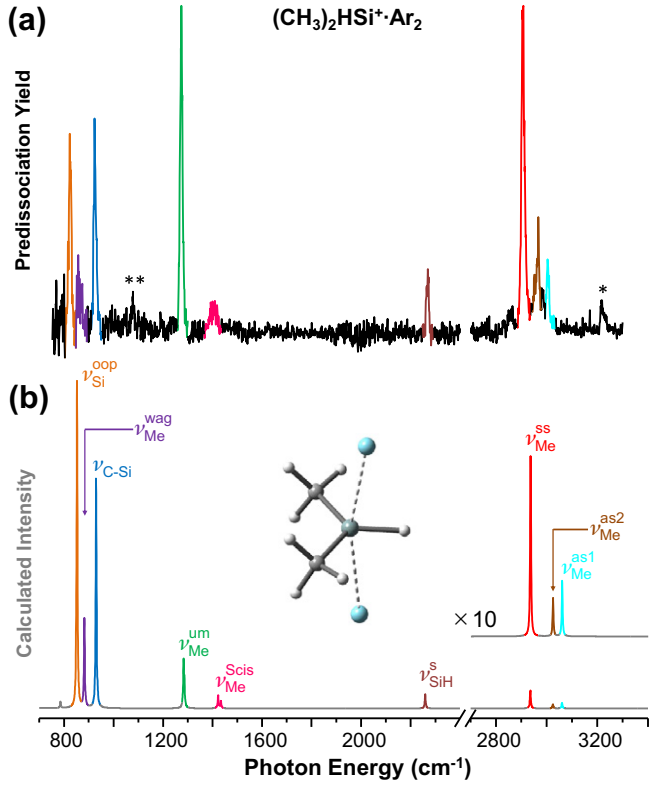

Figure 5. A comparison between the argon predissociation spectrum of $(CH_3)_2HSi^+\cdot Ar_2$ monitoring the photofragmentation of one argon atom (a, black trace) and the *ab initio* harmonic spectrum calculated at the MP2/aug-cc-pVDZ level (b, grey trace, scaled by 0.959 above 2200 cm^{-1}). Vibrations are color coded according to their corresponding fundamentals in the calculated spectrum: silicon out-of-plane bend (ν_{Si}^{oop}, orange), methyl wagging (ν_{Me}^{wag}, violet), Si–C stretching (ν_{C-Si}, blue), methyl umbrella bending (ν_{Me}^{um}, green), methyl scissoring (ν_{Me}^{Scis}, pink), methyl symmetric stretching (ν_{Me}^{ss}, red), SiH stretching (ν_{SiH}^{s}, maroon), type-1 methyl asymmetric stretching (ν_{Me}^{as1}, teal), and type-2 methyl asymmetric stretching (ν_{Me}^{as2}, brown). Experimental spectra are normalized to the most intense transition above and below 1500 cm^{-1}, while calculated spectra are magnified 10× in the CH stretching region. The asterisk (∗) marks a feature that had a relative intensity that varied with subtle changes in source conditions and could be due to an isomer present in small and variable yield or a mass degenerate impurity, perhaps containing oxygen (e.g., $[CH_2SiOH]^+$) which might come from reaction of the silane species with an oxygen-containing impurity such as H_2O. The double asterisk (∗∗) marks a very weak feature that was not recovered by harmonic level calculations, and candidates for its assignment include an overtone or combination band of the silyl or a contribution associated with a mass degenerate impurity (similar to ∗). (For interpretation of the references to color in this figure legend, the reader is referred to the web version of this article.)

(i.e. HCH bending) is clearly evident between 1370 and 1430 cm^{-1}. Not surprisingly, the low frequency vibrations between 800 and 1000 cm^{-1} that arise from displacement of the Si atom are also somewhat different in the two compounds because of the contribution from SiH bending. These result in the orange, violet, and blue bands that are most easily described as Si out-of-plane bending (ν_{Si}^{oop}), methyl wagging (ν_{Me}^{wag}), and Si–C stretching (ν_{Si-C}) motions, respectively.

3. Conclusions

The vibrational predissociation spectra of silyl cations $(CH_3)_2RSi^+\cdot Ar_n$, (R = H and CH_3, n = 1 and 2) have been obtained to reveal the intrinsic infrared signature of these reactive species with weakly interacting ligands (Ar). The spectra down to 800 cm^{-1} were accessible for the di-adducts of both complexes in a linear action regime, which is possible due to the significantly lower binding energy of the second Ar atom. In all cases, the experimental spectra are readily assigned based on agreement with harmonic predictions, thus revealing the remarkably simple intrinsic vibrational mechanics of these ions, which have been resistant to characterization using standard chemical analysis techniques.

Acknowledgements

M.A.J. would like to thank the National Science Foundation for funding under grant CHE-1213634. For performance of *ab initio* calculations, this work was supported in part by the facilities and staff of the Yale University Faculty of Arts and Sciences High Performance Computing Center, and by the National Science Foundation under grant #CNS 08-21132 that partially funded acquisition of the facilities.

References

[1] W.S. Julian Chojnowki, Adv. Organomet. Chem. 30 (1990) 243.
[2] H. Cicak, Kem. Ind. 59 (2010) 111.
[3] J.M. Ruiz, C.F. Guerra, F.M. Bickelhaupt, J. Phys. Chem. A 115 (2011) 8310.
[4] O. Dopfer, Int. Rev. Phys. Chem. 22 (2003) 437.
[5] M.A. Duncan, J. Phys. Chem. A 116 (2012) 11477.
[6] R.V. Olkhov, S.A. Nizkorodov, O. Dopfer, J. Chem. Phys. 108 (1998) 10046.
[7] N. Solca, O. Dopfer, Chem. Phys. Chem. 6 (2005) 434.
[8] G.E. Douberly, A.M. Ricks, B.W. Ticknor, J. Am. Chem. Soc. 129 (2007) 13782.
[9] G.E. Douberly, A.M. Ricks, P.v.R. Schleyer, M.A. Duncan, J. Phys. Chem. 128 (2008). 021102/021101.
[10] M. Okumura, L.I. Yeh, Y.T. Lee, J. Chem. Phys 83 (1985) 3705.
[11] P. Ayotte, G.H. Weddle, J. Kim, M.A. Johnson, Chem. Phys. 239 (1998) 485.
[12] M.A. Johnson, Encyclopedia of Mass Spectrometry, vol. 5, Elsevier, Amsterdam, Boston, 2002.
[13] K. Hiraoka, I. Kudaka, S. Yamabe, Chem. Phys. Lett. 178 (1991) 103.
[14] A. Patzer, S. Chakraborty, O. Dopfer, Phys. Chem. Chem. Phys. 12 (2010) 15704.
[15] M.W. Crofton, M.F. Jagod, B.D. Rehfuss, W.A. Kreiner, T. Oka, J. Chem. Phys. 88 (1988) 666.
[16] J. Dyke, E. Lee, A. Morris, J. Chem. Soc. Faraday Trans. 2 (72) (1976) 1385.
[17] R.R. Holmes, Chem. Rev. 90 (1990) 17.
[18] Z.W. Xie, J. Manning, R.W. Reed, R. Mathur, P.D.W. Boyd, A. Benesi, C.A. Reed, J. Am. Chem. Soc. 118 (1996) 2922.
[19] J.B. Lambert, Y. Zhao, Angew. Chem. Int. Ed. Engl. 36 (1997) 400.
[20] H. Cicak, H. Vancik, Z. Mihalic, J. Org. Chem. 75 (2010) 6969.
[21] J.M. Dyke, N. Jonathan, A. Morris, A. Ridha, M.J. Winter, Chem. Phys. 81 (1983) 481.
[22] J. Berkowitz, J.P. Greene, H. Cho, B. Ruscic, J. Chem. Phys. 86 (1987) 1235.
[23] R.D. Johnson, J.W. Hudgens, J. Chem. Phys. 94 (1991) 5331.
[24] D.M. Smith, P.M. Martineau, P.B. Davies, J. Chem. Phys. 96 (1992) 1741.
[25] M. Savoca, J. Langer, O. Dopfer, Angew. Chem. Int. Ed. 51 (2012) 1.
[26] M. Savoca, M.A.R. George, J. Langer, O. Dopfer, Phys. Chem. Chem. Phys. (2012), http://dx.doi.org/10.1039/C2CP43773B (advance article).
[27] W.C. Wiley, I.H. McLaren, Rev. Sci. Instrum. 26 (1955) 1150.
[28] W.H. Robertson, J.A. Kelley, M.A. Johnson, Rev. Sci. Instrum. 71 (2000) 4431.
[29] A.J. Stace, J. Phys. Chem. – US 91 (1987) 1509.
[30] A.J. Stace, D.M. Bernard, Chem. Phys. Lett. 146 (1988) 531.
[31] C.E. Klots, J. Chem. Phys. 83 (1985) 5854.
[32] M.J. Frisch, G.W. Trucks, H.B. Schlegel, G.E. Scuseria, M.A. Robb, J.R. Cheeseman, G. Scalmani, V. Barone, B. Mennucci, G.A. Petersson, H. Nakatsuji, M. Caricato, X. Li, H.P. Hratchian, A.F. Izmaylov, J. Bloino, G. Zheng, J.L. Sonnenberg, M. Hada, M. Ehara, K. Toyota, R. Fukuda, J. Hasegawa, M. Ishida, T. Nakajima, Y. Honda, O. Kitao, H. Nakai, T. Vreven, J.A. Montgomery, Jr., J.E. Peralta, F. Ogliaro, M. Bearpark, J.J. Heyd, E. Brothers, K.N. Kudin, V.N. Staroverov, R. Kobayashi, J. Normand, K. Raghavachari, A. Rendell, J.C. Burant, S.S. Iyengar, J. Tomasi, M. Cossi, N. Rega, J.M. Millam, M. Klene, J.E. Knox, J.B. Cross, V. Bakken, C. Adamo, J. Jaramillo, R. Gomperts, R.E. Stratmann, O. Yazyev, A.J. Austin, R. Cammi, C. Pomelli, J.W. Ochterski, R.L. Martin, K. Morokuma, V.G. Zakrzewski, G.A. Voth, P. Salvador, J.J. Dannenberg, S. Dapprich, A.D. Daniels, Ö. Farkas, J.B. Foresman, J.V. Ortiz, J. Cioslowski, and D.J. Fox, Gaussian 09, Revision A.1, Gaussian, Inc., Wallingford CT, 2009.